Sedimentological and geochemical evidence for palaeo-environmental change in the Makgadikgadi subbasin, in relation to the MOZ rift depression, Botswana

Susan Ringrose[a,*], Philippa Huntsman-Mapila[a,b], Ali Basira Kampunzu[c,✠], William Downey[d], Stephan Coetzee[d], Bernard Vink[c], Wilma Matheson[e], Cornelis Vanderpost[a]

[a]*Harry Oppenheimer Okavango Research Centre, University of Botswana, Private Bag 285, Maun, Botswana*
[b]*UBO-CNRS UMR, 6538 Domaine Oceaniques IUEM, 29280 Plouzane, France*
[c]*Department of Geology, University of Botswana, Private Bag 0022, Gaborone, Botswana*
[d]*Department of Physics, University of Botswana, Private Bag 0022, Gaborone, Botswana*
[e]*EES (Pty) Ltd., P.O. Box 31024, Gaborone, Botswana*

Dedicated to the late Professor A.B. Kampunzu whose inspiration will always remain with us.

Abstract

This work considers new evidence for palaeo-environmental change taking place during the Pleistocene in northern Botswana. Duricrusted strandlines along the northeastern margin of Sua Pan provide palaeo-environmental data pertaining to the Makgadikgadi subbasin (MSB) with inferences regarding the larger Makgadikgadi–Okavango–Zambezi (MOZ) rift depression. Field, XRD and geochemical data show that MSB strandlines comprise calcretes (LU1 type), MgO-rich calcretes with silica (LU2 type), sil-calcrete (LU3 type) and silcrete (LU4 type). Early freshwater episodes appear to have been followed by calcrete-dominated drying phases interspersed with repeated silcretisation. Calcretisation through pan littoral sediments may have been both biogenically and environmentally induced. Calcite precipitation was in part controlled by the Mg/Ca ratio of pore water in the pan littoral zone suggesting closed basin type evaporative conditions, which were followed by a major desiccation interval. Phases of silcrete precipitation appear to be related to periods when the geochemistry of the lake littoral more closely resembled present-day Na–CO_3–SO_4–Cl-type brines. Silica saturated acidic, moderately saline groundwater preceded Si precipitation which took place as the pH reduced. Si mobilisation occurred (inter alia) as a result of quartz grain dissolution enhanced by diatoms, bacteria and algal growth in the moist pan littoral. SiO_2-rich pore waters migrated through cracked and desiccated calcrete into areas of lower salinity and lower pH resulting in preferential calcite removal and silcrete precipitation. Approximate TL dates imply that exposed littoral sand underwent calcretisation during the drying phases of extensive palaeo-lakes which occurred prior to 110 ka, 80–90 ka and 41–43 ka. These wet periods compare fairly well with Vostok core chronologies for southern Africa.

Keywords: Silcrete; Calcrete; Palaeo-environmental change; Palaeo-Makgadikgadi subbasin; Biogenic processes

* Corresponding author. Fax: +267 6861835.
E-mail addresses: sue_ringrose@hotmail.com, sringrose@mopipi.ub.bw (S. Ringrose).

✠ We wish to acknowledge the untimely death of Professor Kampunzu and express our gratitude for all his help and support of palaeo-environmental work in Botswana.

1. Introduction

Fluvio-lacustrine deposition in northern Botswana has mainly taken place within a large structural (mega) depression, a southwesterly propagating extension of the east African rift system, which was initiated approximately 2.4–5.0 Ma (Du Toit, 1933; Tiercelin and Lezzar, 2002). This rift depression was drained and filled by southeasterly flowing rivers on a number of occasions during the Tertiary and Pleistocene as the area was faulted and half grabens developed (Cooke, 1980; Mallick et al., 1981; Modisi et al., 2000). Deeper structural subbasins formed mainly on the southern margin of the rift forming loci for lacustrine deposition (Thomas and Shaw, 1991; Gumbricht et al., 2001; Ringrose et al., 2002a). The MOZ (Makgadikgadi–Okavango–Zambezi) depression is controlled by a series of NE–SW normal faults related to incipient rifting which reactivated Proterozoic and Karoo structures (Baillieul, 1979; Smith, 1984; Modisi et al., 2000). Tectonic activity along the same trend resulted in uplift along the Zimbabwe–Kalahari axis possibly during the late Pliocene (Partridge and Maud, 2000; Moore and Larkin, 2001) causing the impoundment of proto Okavango, Kwando and upper Zambezi drainage and the development of the Makgadikgadi (MSB), Ngami and Mababe subbasins (Cooke, 1980; Ringrose et al., 2002b). The MSB comprises two large salt pans referred to as Sua Pan in the east and Ntwetwe Pan in the west covering some 37 000 km^2.

This work considers new approaches to the interpretation of palaeo-lacustrine environments from the Makgadikgadi subbasin (MSB) in the context the MOZ rift depression based on morpho-stratigraphic evidence and thermoluminescence (TL) dates. To avoid confusion, the term Lake Palaeo-Makgadikgadi which was intended to encompass all fluvio-lacustrine events in the nascent rift in the older literature (e.g., Cooke, 1979; Cooke and Verstappen, 1984; Thomas and Shaw, 1991; Ringrose et al., 1999a) is being discontinued, as it suggests an enlarged version of the present Makgadikgadi Pan complex (cf. Moore and Larkin, 2001). Hence, the introduction of the term Makgadikgadi–Okavango–Zambezi (MOZ) rift depression wetlands to help clarify the regional context. The apparent semi-continuous development of palaeo-lakes in the MSB from possibly late Pliocene to Recent times has been subject to speculation especially with respect to the nature of feeder channels and links to the Okavango system. Results of previous work have mainly been based on height data from assumed strandlines with minimum age ^{14}C dates (Cooke and Verstappen, 1984; Thomas and Shaw, 1991, 2002; Ringrose et al., 1999a). The present work emphasises duricrust strandline morphogenesis from the northeastern MSB to help interpret depositional environments. This takes place in the context of new indicative thermoluminescence (TL) dates which are used to amplify geochronological events. Specific aims include the development of morpho-stratigraphic records and the establishment of geochemical units intended to develop innovative data for palaeo-environmental change. Strandline evolution in terms of MSB and MOZ depression palaeo-environments is further elaborated.

2. Study area

The study area forms part of the northeastern Makgadikgadi subbasin in north central Botswana between 19.80 S–21.60 S and 25.75 E–26.40 E covering approximately 3600 km^2 (Fig. 2). Background geology comprises Archean terrain covered by >250 m of Karoo sediment (Lebung and Ecca Groups) crossed by the Okavango dyke swarm including Proterozoic and Jurassic mafic dykes (Geological Survey of Botswana, 2000). These in turn are covered by Kalahari Group sediments (Mallick et al., 1981).

The development and subsequent enlargement of the MSB appears to have resulted from downwarping at the intersection of NE–SW nascent rift structural trends with orthogonal NW–SE Karoo trends (Fig. 1). A significant feature in the study area is Sua Spit, which in common with other remnant linear features in the MSB follows NW–SE trends. Sua Pan is infilled with clay, silt and fine sand currently saturated by a near surface brine aquifer of the Na–CO_3–SO_4–Cl type (Eugster and Hardie, 1978; Shaw et al., 1990). Sua Pan is the lowest member of the Pan sequence with a sump level of 890 m a.s.l. The area is sparsely vegetated with anomalously low rainfall at c. 400 mm/year (Ringrose et al., 1999b). The precipitation rate is exceeded by the evapotranspiration rate by a factor of three (Bhalotra, 1987).

3. Analytical techniques

Field work at three locations took place between 1999 and 2002 and was aimed at characterising duricrusts throughout the known range of strandline levels. Observational data and samples were taken from twenty gravel pits and road cuts in Location 1, ten hand dug pits in Location 2 and five gravel pits in Location 3 (Fig. 2). Satellite images provided a basis for the selection of northwest–southeast and north–south transects which were used to establish topographic profiles and the locations for duricrust examination. Topographic profiling took place to fit the strandlines into the existing height-based geochronology. For this, a Trimble 4700 differential GPS was used in Location 1. Topographic data for Locations 2 and 3 were obtained from topographic maps and survey beacons the heights of which were available from the Botswana Department of Surveys and Mapping. Additional contour data were obtained from the Makgadikgadi Pans Development Plan (Republic of Botswana, 2000). Field methods included the clearing of pit faces, their differentiation into sedimentary units, the development of a systematic field description following terminology available in Wright and Tucker (1991) and the sampling of all major units and plant remains. Units intended for TL analysis were covered by a tarpaulin and sampled in the dark. Samples comprised large coherent mega-aggregates which were dug from the interior of the pit wall, covered immediately in aluminium foil and placed in a lightproof plastic container. A series of samples were taken from each location intended to be representative of older litho-clasts, intermediate indurated and younger friable nodular horizons. Samples were taken from homogeneous horizons, representative of material supplying the environmental dose rate. Twenty duricrust samples were sent to the Council for Geoscience, Pretoria for thin sectioning. The thin sections were later investigated under plain and cross-polarised light using a Zeiss Axioplan microscope. A Philips XL30 environmental scanning electron microscope (ESEM) with an electron microprobe (EDAX) was used to obtain preliminary micro-textural information, to determine the nature of microorganisms and to provide localised qualitative elemental data. Naturally occurring surfaces were examined without preparatory polishing to preserve micro-textures.

Twenty bulk samples were subject to X-ray diffraction powder analysis using a Phillips PW 3710 XRD unit, operated at 45 kV and 40 mA, employing Cu-K alpha radiation and a graphite monochronomator. The samples were scanned from 3° to 70° 2θ and their diffractograms recorded. After initial scanning, the bulk samples were leached in a dilute 10% HCl solution. The leached residues were scanned for minor and accessory insoluble silicate phases. Whole rock chemical analyses were performed on twenty-five samples at Chemex Laboratories (Canada). Major element compositions were determined using an ICP-AES with a detection limit of 0.01 wt.% and precision of ±1%. Inorganic CO_2 and organic C were determined using a Leco-Gasometric and Leco-IR detector with detection limits of 0.2 and 0.01, respectively.

Eleven samples were dated using TL techniques (Aitken, 1985). This technique was used because it has provided reliable dates in the past (Blumel et al., 1998; Ringrose et al., 1999a, 2002a,b). Literature sources suggest a degree of comparability between TL and OSL (optical spin luminescence) (e.g., Radtke et al., 1999; Huaya et al., 2004). Quartz grains in the size range 90–125 μm, assumed to have undergone total bleaching in a shallow water environment before duricrust precipitation, were extracted from litho-clasts and nodules using a series of treatments. These included removal of carbonates

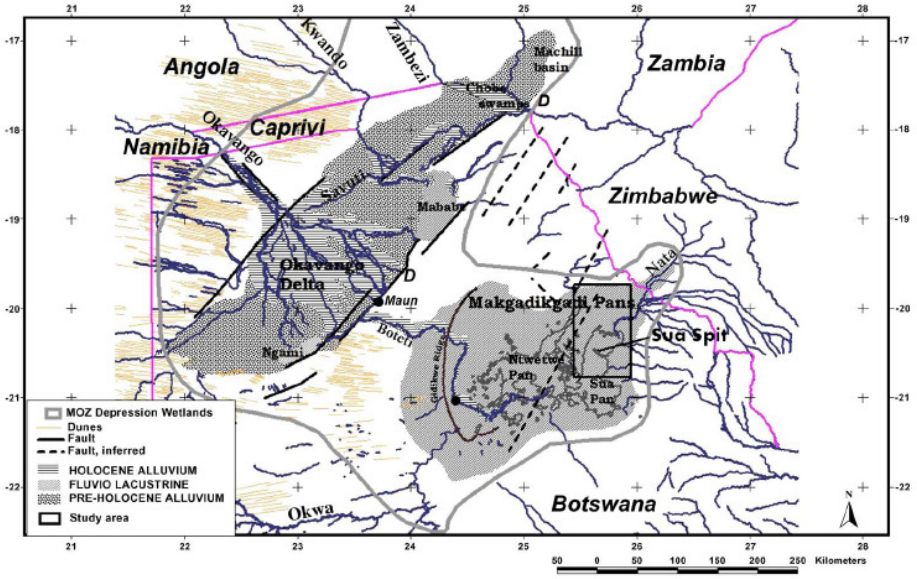

Fig. 1. Location of the palaeo-Makgadikgadi subbasin (MSB) in relation to the Makgadikgadi–Okavango–Zambezi (MOZ) rift depression (D=location of TL date sites).

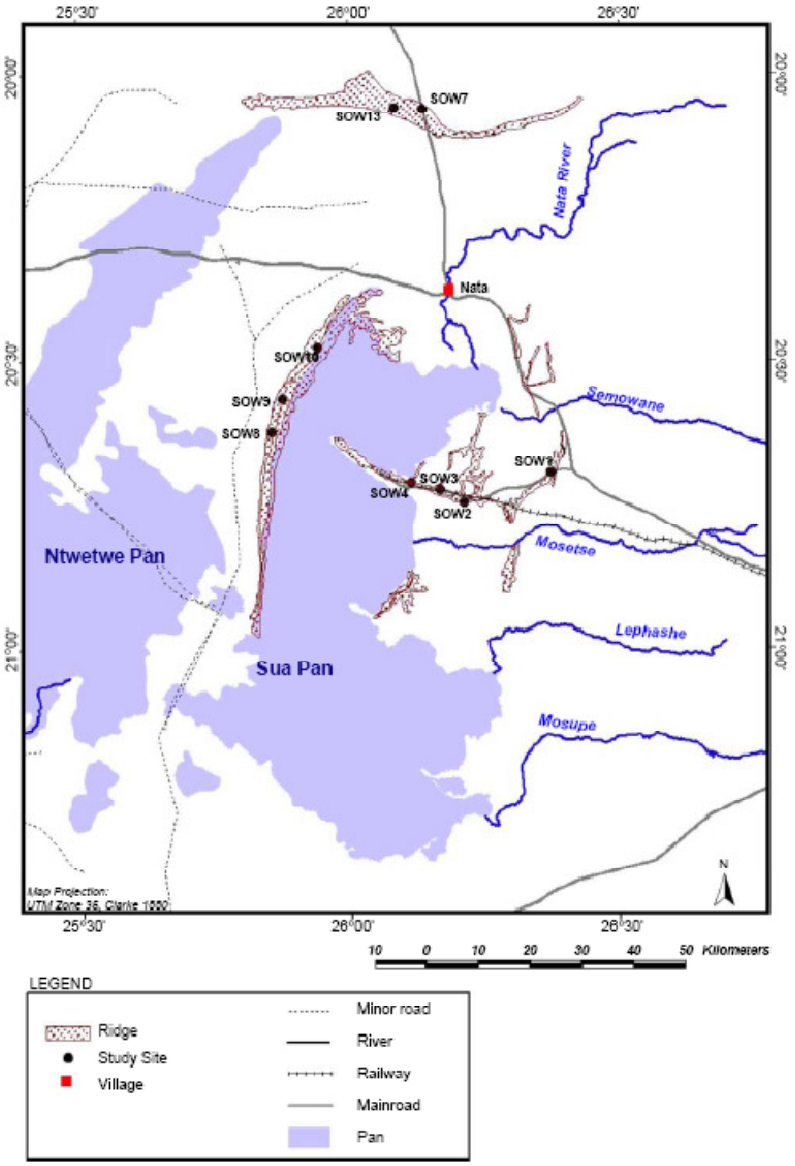

Fig. 2. Study area and sample locations on the northeastern margin of the palaeo-Makgadikgadi subbasin.

and iron staining using hydrochloric acid and digestion of organic material using hydrogen peroxide. Fluorosilicic acid was used to dissolve feldspars while heavy minerals were separated using sodium polytungstate. Remaining magnetic minerals were removed using an electromagnetic separator. The purity of the final quartz extract was tested using Infrared Stimulated Luminescence to ensure that no feldspars were present. The clean sample was subjected to a hydrofluoric acid etch for 40 min at 24 °C to remove the outer α affected skin. The grains were mounted on 10-mm-diameter stainless steel discs and fixed using Silkospray silicone oil. Multiple aliquots were used for each additive dose step and regenerated bleached samples. The strontium 90 β source was calibrated against a known β source to deliver 1.9 Gy min^{-1}. Additive doses +β1, +β2 etc. in Gy were used for natural and bleached samples (Table 1). Following the appropriate irradiations, the sample was stored for 24 h and preheated at 220 °C for 300 s before TL measurement using a Riso D12 reader (Botter-Jensen and Duller, 1992). A second glow normalisation was performed on the glowed out samples using a dose of 6 Gy for each sample. The TL glow curves show convincing temperature plateaux over the temperature ranges (Table 1). Exponential regressions for TL in relation to Dose were performed for each sample and the equivalent dose (DE) obtained from which the residual TL was subtracted. The TL data were fitted by exponential regression over the best temperature plateau range for both the additive dose and bleached regenerated data and a comparison made of the respective curve forms. In this case, the R^2 regenerated TL growth curve coefficient was within an acceptable range. The environmental dose rate was determined by a low-level alpha counter (Elsec 7286) using a 42-mm ZnS screen (Zoller and Pernicka, 1989). The values shown assume secular equilibrium for both U and Th chains (Carl, 1987). Uncertainty levels on Table 1 represent one standard deviation. The potassium content (wt.%) was determined using a Corning 410 flame photometer. The moisture value used in the age equation determination of these samples is 5%±5%. The cosmic dose was calculated taking into consideration depth of burial, overburden density and porosity, sample coordinates and altitude.

Table 1
Data inputs for thermoluminescence analysis (see text for explanation)

Sample	SOW13S2P	SOW13S1	SOW13S3	SOW13S2A	SOW7AS2	SOW13S2	SOW1 S6	SOW4 S4	SOW8A	MAUNSE12A	KVFS3
Sample (De)(Gy)	86.77±0.79	164.851±81	118.78±6.71	72.37±1.79	157.83±15.28	50.02±1.24	219.83±7.20	111.57±9.00	48.66±3.81	337.50±16.90	666.00±33.30
Sediment U ppm	0.92±0.09	1.92±0.19	1117±0.62	1.02±0.15	0.75±0.05	110±90.09	811 2±0.26	0.80±0.09	15.73±0.61	1.33±0.18	0.93±0.09
Sediment Th ppm	1.73±0.30	4.14±0.62	4.60±0.62	2.57±0.48	1.14±0.18	1.37±0.28	1.47±0.86	0.92±0.28	16.18±2.03	6.00±0.58	1.47±0.28
K wt.%	0.32±0.03	0.740±.03	0.58±0.03	0.30±0.03	1.58±0.03	0.74±0.03	0.28±0.03	2.28±0.33	0.54±0.03	2.00±0.03	1.00±0.03
Dose rate mGya^{-1}	799±66	1613±119	1313±106	866±79	1956±118	1213±84	2423±174	2570±162	5560±401	2813±178	1350±93
Plateau (Temp. range °C)	319–354	316–411	296–365	303–354	328–399	331–435	307–345	334–376	314–377	–	–
Additive dose +b1(Gy)	116.67	33.33	66.67	100	100	26.67	133.33	26.67	26.67	–	–
+b2	233.33	66.67	100	166.67	200	66.67	283.33	166.67	56.67	–	–
+b3	333.33	266.67	150	266.67	533.33	233.33	500	266.67	100	–	–
+b4	–	–	366.67	–	–	–	–	–	166.67	–	–

4. Topographic, stratigraphic and petrographic results

Location 1 ridges were examined at eleven locations and in detail at exposures SOW1 to SOW4 (Fig. 2). The Pan floor immediately adjacent to Sua Spit lies at an elevation of 904 m and rises up through a series of minor sand and duricrust ridges, the most prominent of which lie at 906 m and 908 m. The exposures examined in detail occur immediately landward of the Spit such that SOW4 stands at 911 m, SOW3 at 924 m SOW2 at 926 m and SOW1 at 936 m. While the lowest unit in the upper SOW1 ridge is an indurated, calcareous lithoclastic bed showing desiccation cracking, the lowest units in the remaining profiles (SOW2–4) comprise well-developed (3–5 cm) rhyzoliths in a green, granular calcareous matrix (Fig. 3). The rhyzoliths appear to be root casts (sensu Klappa, 1980) in units which also contain small litho-clasts showing desiccation cracking and void formation. The rhyzoliths are large, up to 1–2 cm in diameter and 8–10 cm long, comprising a greenish-white calcareous exterior (1–2 mm) and grey-brown siliceous interior (Fig. 4A). This unit grades upwards into moderately indurated nodular calcrete with cracked siliceous litho-clasts in a partially indurated sandy calcareous matrix. The nodules are small and composed of concentric shells of $CaCO_3$ accreted around quartz or calcite nuclei and occur more towards the top of the unit, while the litho-clasts are larger (1–3 cm) and more angular. In SOW2 and 3, the nodules grade upwards into a more friable, nodular calcrete. In SOW4, the nodular litho-clastic unit is replaced vertically by calcareous siltstone showing major desiccation cracking (Fig. 4B) succeeded by honeycomb calcrete which in turn is capped by an indurated, calcareous hardpan comprising calcareous litho-clasts (Fig. 3). SOW2, 3 and 4 are capped by indurated, calcrete hardpan with calcareous and siliceous litho-clasts. In contrast, the higher SOW1 units comprise lower laminar calcrete which is rhyzolith free and succeeded by a calcareous siltstone showing major desiccation cracking. This is overlain by friable, nodular calcrete and capped by conglomeratic hardpan made up of indurated duricrust comprising either large (0.5–3.0 cm) quartz and calcrete clasts in a micritic, partially Fe-stained matrix. The conglomeratic quartz clasts show evidence of vertical and peripheral cracking in addition to Fe staining.

A series of ridges were examined Location 2 adjacent to the west side of Sua Pan, in detail at the indurated SOW10 ridge. The Pan floor west of Sua Spit lies at an elevation of about 900 m and rises up through a series of lower sand ridges to more prominent duricrust ridges at 904 m and 906 m. The SOW10 906 m ridge is completely lithified and comprises three units (Fig. 3). The lower unit is composed of recrystallised green calcrete with calcareous and siliceous litho-clasts showing extensive cracking. The siliceous litho-clasts are lensoid (terrazzo) in shape with notable Fe staining (Fig. 4C). The intermediate unit is made up of brecciated silcalcrete litho-clasts in an indurated calcareous matrix with voids and desiccation cracking throughout. The upper unit is composed of indurated calcareous sediment with severely cracked sub-rounded green litho-clasts showing laminar to massive infilling. Lower Location 2 sand ridges rise up 1–3 m from the western edge of Sua Pan. The sandy ridges, examined at SOW8B comprise 0.5 m uniform sand with disseminated calcareous particles and scattered rhyzoliths. A series of silica-rich lensoid terrazo plates are present along the former shoreline. These plates vary in length from 2 to 10 cm and are 1–3 cm in thickness and lie on the present pan edge in random discontinuous sheets (Fig. 4D).

SOW7A and 13 occur in Location 3 on the northeastern margin of the Makgadikgadi Basin at around 943–945 m (Fig. 2). In terms of height and lateral continuity, ridges at this elevation have been described as representing the oldest strandline features in the PMSB (Thomas and Shaw, 1991). The basal bed of SOW7A comprises an indurated litho-clastic unit with sub-rounded quartz clasts in a hardened calcareous matrix (S5, Fig. 3). In contrast, the basal unit of SOW13 (S4, Fig. 3) is made up of semi-consolidated light green sand with calcareous fragments and fine quartz particles interspersed with rhyzoliths. Both lower units are replaced by partially indurated nodular calcrete with siliceous, angular, large (to 4 cm) litho-clasts showing evidence of desiccation cracking. This is succeeded in both profiles (SOW13 and 7A) by friable nodular calcrete with abundant rhyzoliths. The rhyzoliths are mostly large (up to 3.5 cm diameter and 2–6 cm long)

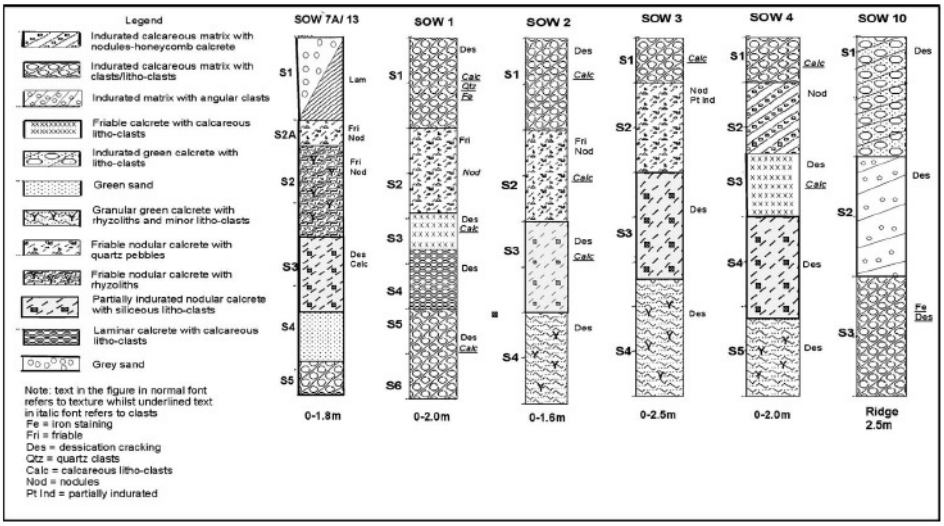

Fig. 3. Stratigraphic profiles of duricrusts in the three sample locations (SOW1–4=Location 1, SOW 10=Location 2, SOW7A and SOW 13=Location 3).

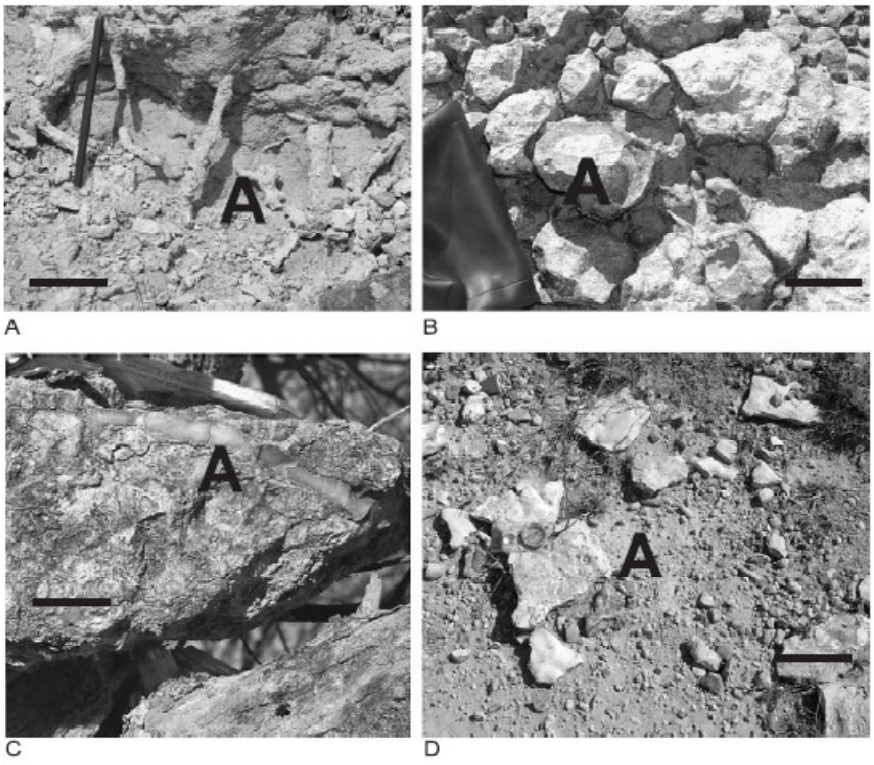

Fig. 4. (A) Numerous rhyzoliths (A) in green, granular calcareous matrix at SOW3 S4 (bar=6 cm). (B) Dessication cracking showing alteration of $CaCO_3$-rich pebbles (A) by silica rich pore water SOW4 S3 (bar=10 cm). (C) Lensoid terrazzo plates congealed in the SOW10 ridge (bar=5 cm). (D) Lensoid terrazzo plates along the edge of Sua Pan near SOW10 (bar=8 cm).

comprising calcareous outer sheaths with a siliceous infilling. This unit grades upwards into a friable nodular bed with quartz clasts. The nodules are mainly composed of quartz nuclei with carbonate rich concentric outer shells. The profiles are capped by a massive calcareous hardpan in SOW13 and massive grey sand in SOW7. The hardpan comprises lenticular siliceous clasts in a calcareous matrix.

5. X-ray diffraction and geochemical results

XRD analyses of litho-clastic and nodular samples indicate that the MSB duricrusts may be subdivided into calcite- or quartz-dominated types (Table 2). In Location 1 SOW1, calcite (or calcite with dolomite) is dominant and varies from 66 vol.% to 80 vol.% calcite down profile. More quartz clasts are found in the upper units. The presence of feldspars is low at 1–2 vol.% microcline and albite, despite the proximity of Karoo bedrock. The proportion of dolomite (3–4 vol.%) and the presence of palygorskite (3–8 vol.%) with sepiolite (2–8 vol.%) confirm the prevalence of Mg in the strandline duricrusts. The presence of Mg-rich clays and dolomites suggests formation in Mg-rich alkaline environments, normally associated with a closed basin depositional history (e.g., Watts, 1980; Eugster and Kelts, 1983; Alonso-Zarza et al., 2002).

Table 2
Results of X-ray diffraction analysis (vol.%) on selected MSB strandline sediments

SAMPLE	Cal	Dol	Qtz	Mcl	Alb	Mca	Pal	Sep	Ill	Cly	Mag	Ken	Hem	Hal
SOW 1-S1	66	3	23	2	<1	–	4	–	–	–	–	–	–	–
SOW 1-S2	72	4	18	1	2	<1	–	–	–	–	–	–	–	–
SOW 1-S3	74	5	13	1	1	–	3	2	–	–	–	–	<1	–
SOW 1-S4	65	5	18	2	1	–	8	–	–	–	–	–	–	–
SOW 1-S5	62	4	13	3	2	–	7	8	–	–	–	–	–	–
SOW 1-S6	80	–	14	<1	<1	–	5	–	–	–	–	–	–	–
SOW 3-S1	43	10	36	4	6	2	–	–	–	–	–	–	–	–
SOW 3-S2	9	42	36	5	3	–	–	–	–	4	–	–	–	–
SOW 3-S3	36	7	45	5	4	–	–	–	–	–	–	–	<1	–
SOW 3-S4	47	–	30	6	3	–	–	–	12	–	–	–	–	–
SOW 7A-S1	<1	–	88	5	1	–	–	–	5[a]	–	–	–	–	–
SOW 7A-S2	30	15	50	2	<1	–	–	–	3[a]	–	–	–	–	–
SOW 7A-S2A	18	2	70	5	1	–	–	–	–	4	–	–	–	–
SOW 7A-S3	2	–	82	5	1	–	–	–	10	–	–	–	–	–
SOW 7A-S4	64	–	22	2	1	–	–	–	12[a]	–	–	–	–	–
SOW 8A	40	–	33	3	4	–	–	–	–	–	10	10	–	–
SOW 8B	24	–	40	2	3	–	–	–	–	–	15	15	–	–
SOW 10-S1	44	2	45	1	1	–	–	–	2	6	–	–	–	–
SOW 10-S2	22	–	72	2	1	–	–	–	4	–	–	–	–	–
SOW 10-S3	74	–	18	1	<1	–	–	–	7	–	–	–	–	–
SOW 13-S1	30	–	52	4	3	–	–	10	–	–	–	–	–	–
SOW 13-S1A	60	–	20	<1	1	–	–	14	–	–	–	–	–	–
SOW 13-S2	8	–	65	5	5	–	–	15	–	–	–	–	–	2
SOW 13-S2A	10	38	42	3	1	–	–	–	3	–	–	–	–	–

Cal=Calcite, Dol=dolomite, Qtz=quartz, Mcl=microline, Alb=albite, Mca=micas, Pal=palygorskite, Sep=sepiolite, Ill=Illite, Cly=clay minerals, Mag=magadiite, Ken=kenyaite, Hem=hematite, Hal=halite.
[a] Approximate quantities.

Results from SOW3 litho-clasts and nodules show a more even proportion of calcite (9–47 vol.%) and quartz (30–45 vol.%). Mg is abundant throughout with the S2 unit containing 42 vol.% dolomite. The proportion of feldspars is slightly higher than that found in SOW1 at 4–6 vol.% microcline and 3–6 vol.% albite. The presence of illite (3–12 vol.%) or possibly glauconite contrasts with the palygorskite and sepiolite found in SOW1 and may be detrital in origin.

On the western side of Sua Pan at Location 2, the ridge at SOW10 comprises an even proportion of calcite and quartz with minor dolomite (2 vol.%) towards the top of the ridge, higher quartz (72 vol.%) about halfway down and higher calcite (74 vol.%) towards the ridge base (Table 2). The feldspar proportion is low throughout. The percentage of illite (or glauconite) increases towards the base (from 2 to 7 vol.%). Watts (1980) discusses how glauconite is lost during calcretisation as glauconite and calcite are incompatible (cf. Krumbein and Garrels, 1952). The pan edge duricrusts (SOW8A/8B) show relatively equal proportions of quartz (33–40 vol.%) and calcite (24–40 vol.%) with intermediate feldspars. Two samples contain relatively high proportions of magadiite and kenyaite whose presence implies that the pan littoral was exceptionally alkaline and saline during their formation. Both minerals are considered to have formed from a reaction between dissolved halite and silica (Vink et al., 2001).

Towards the northern edge of the basin at SOW7A, XRD analysis on litho-clasts and nodules shows that high calcite concentrations (64 vol.%) towards the base become lower (to <1 vol.%) towards the top of the profile while the reverse is true for quartz (89–22 vol.%). An exceptional unit to this trend is SOW7A which shows high quartz and low calcite towards the base of the profile (Table 2). Most units contain 3–12 vol.% clay which may be either detrital illite or glauconite and a low feldspar content. A relatively high dolomite percentage (15 vol.%) occurs towards

the top of the profile at SOW7A S2. SOW13 also comprises dolomite (38 vol.%) towards the top of the profile in association with a variable quartz (20–66 vol.%) and calcite (8–60 vol.%) content. The SOW13 samples contain a high proportion of neoformed sepiolite (10–15 vol.%). The Mg-rich mineral suite implies neoformation of clays and dolomite likely under alkaline rich, closed basin conditions (Watts, 1980; Eugster and Kelts, 1983).

Geochemical results from twenty nodular and litho-clast samples indicate a high correlation between $CaCO_3$ and SiO_2 (R^2=0.985) suggesting inverse precipitation trends (cf. Gwosdz and Modisi, 1983) and the incompatibility of precipitation environments of these two elements (Thomas and Shaw, 1991). AlO_2 and $Fe2O_3$ are also correlated (R^2=0.751) along with SiO_2 and TiO_2 at R^2=0.617 implying that most silicates are derived from Precambrian bedrock sources as a result of weathering and transportation. There is no correlation between $CaCO_3$ and MgO or between SiO_2 and MgO. Results indicate high LOI values (>30 vol.%) in the SOW1, SOW7A S4 and SOW10 S3 implying a high carbon content for these calcretes (Table 3). Geochemical results along with XRD data indicate that the MSB duricrusts may be subdivided into four subgroups broadly following classifications proposed by Walker (1960), Summerfield (1983a,b) and Nash and Shaw (1998). Litho-unit $CaCO_3$ and SiO_2 proportions in relation to profile heights and duricrust type are shown on Table 4. Specifically, litho-unit 1 (LU1) is banded between 60–80 wt.% calcite and 10–30 wt.% SiO_2 and is referred to as calcrete (Fig. 5). While examples of LU1 are present at all locations, the high calcite litho-unit is found mainly at 936 m in Location 1, SOW1. Litho-unit 2 (LU2) is banded between 35–50 wt.% calcite and 35–52 wt.% SiO_2, and composed of approximately equal proportions of calcite and siliceous sediment. This is referred to as calcrete with silica. LU2 duricrusts occur throughout the study area but are found mainly around 924 m (SOW3). Litho-unit 3 (LU3) is banded between

Table 3
Major element composition in vol.% in relation to morpho-stratigraphic sequence from MSB strandlines (missing are Cr_2O_3 at 0.01 vol.% for all samples and MnO ranging from 0.01 to 0.09 for all samples)

Sample	K_2O	Al_2O_3	CaO	Fe_2O_3	MgO	Na_2O	P_2O_5	TiO_2	CO_2inorg %	LOI
SOW 1-S1	0.33	1.5	37.74	0.66	1.96	0.15	0.01	0.09	29.6	32.73
SOW 1-S2	0.3	1.11	41.19	0.6	1.92	0.17	0.03	0.06	31.8	35.6
SOW 1-S3	0.2	0.67	42.96	0.31	3.21	0.17	0.05	0.05	33.6	38.65
SOW 1-S4	0.3	1.12	36.57	0.47	3.71	0.2	0.04	0.08	31	34.39
SOW 1-S5	0.38	1.42	35.62	0.49	4.72	0.23	0.01	0.08	28.8	33.55
SOW 1-S6	0.31	1.11	42.67	0.46	1.84	0.15	0.01	0.06	33.6	36.47
SOW 3-S1	0.78	2.03	25.16	0.62	4.08	0.4	0.01	0.08	22.8	25.05
SOW 3-S2	1.06	3.06	17.86	0.87	9.38	0.65	0.01	0.12	22.8	24.73
SOW 3-S3	1.02	2.68	19.95	0.66	4.87	0.52	0.01	0.1	17.8	21.75
SOW 3-S4	0.94	2.43	26.5	0.65	4.26	0.5	0.01	0.11	22.4	26.21
SOW 10-S1	0.76	1.29	25.92	0.5	0.82	0.23	0.27	0.09	20	23.11
SOW 10-S2	1.1	1.84	12.18	0.69	0.71	0.2	0.03	0.1	10	11.22
SOW 10-S3	0.65	1.03	41.29	0.42	0.98	0.14	0.03	0.05	32.6	34.37
SOW 8A	0.74	1.64	21.79	0.47	1.14	1.95	0.01	0.08	17	22.05
SOW 8B	0.7	1.78	13.35	0.53	1.53	2.68	0.01	0.08	9.6	17.92
SOW 7A-S1	0.92	2.18	0.24	0.68	0.43	0.16	0.01	0.14	0.2	2.09
SOW 7A-S2	0.94	1.94	21.33	0.68	3.55	0.18	0.01	0.09	18.6	20.95
SOW 7A-S2A	0.92	2.02	10.39	0.61	2.01	0.14	0.01	0.1	8.6	11.04
SOW 7A-S3	1.64	3.35	1.11	1.23	2.05	0.2	0.01	0.15	0.8	3.79
SOW 7A-S4	1.11	1.77	36.3	0.75	1.18	0.14	0.03	0.08	28.2	30.77
SOW 13-S1	0.85	2.07	16.94	0.72	3.09	0.26	0.01	0.15	13.2	17.79
SOW 13-S1A	0.54	1.26	33.87	0.47	3.53	0.21	0.03	0.08	26	31.5
SOW 13-S2	0.87	1.72	4.63	0.63	3.43	1.03	0.01	0.16	3.4	10.27
SOW 13-S2A	0.5	1.09	18.15	0.39	9.09	0.21	0.01	0.11	21.8	25.1
SOW 13-S3	0.87	1.85	13.43	0.68	2.19	0.14	0.01	0.16	9.6	13.64

Table 4
Duricrust type and calcite–silica compositon (vol.%) in relation to morpho-stratigraphic sequence from MSB strandlines

Sample	Height m a.s.l.	$CaCO_3$ SiO_2	Litho-unit	Duricrust type
SOW 1-S1	936	67.32	25.6	1 Calcrete
SOW 1-S2	936	72.32	19.24	1 Calcrete
SOW 1-S3	936	76.41	14.09	1 Calcrete
SOW 1-S4	936	70.5	23.64	1 Calcrete
SOW 1-S5	936	65.5	24.34	1 Calcrete
SOW 1-S6	936	76.41	17.15	1 Calcrete
SOW 3-S1	924	51.85	42.47	2 Calcrete with silica
SOW 3-S2	924	51.85	42.16	2 Calcrete with silica
SOW 3-S3	924	40.48	48.88	2 Calcrete with silica
SOW 3-S4	924	50.94	38	2 Calcrete with silica
SOW 7A-S1	943–945	0.45	93	4 Silcrete
SOW 7A-S2	943–945	42.3	50.9	2 Calcrete with silica
SOW 7A-S2A	943–945	19.56	72.56	3 Sil-calcrete
SOW 7A-S3	943–945	1.82	86.09	4 Silcrete
SOW 7A-S4	943–945	64.13	28.16	1 Calcrete
SOW 8A	905	38.66	50.87	2 Calcrete with silica
SOW 8B	908	21.83	62.03	3 Sil-calcrete
SOW 10-S1	910	45.48	47.16	2 Sil-calcrete
SOW 10-S2	910	22.74	72.5	3 Sil-calcrete
SOW 10-S3	910	74.14	20.83	1 Calcrete
SOW 13-S1	943–945	30.02	58.68	3 Sil-calcrete
SOW 13-S1A	943–945	59.13	29.03	2 Calcrete with silica
SOW 13-S2	943–945	7.73	78.46	3 Silcrete
SOW 13-S2A	943–945	49.58	46.02	3 Sil-calcrete
SOW 13-S3	943–945	21.83	67.03	4 Silcrete

15–30 wt.% calcite and 58–72 wt.% SiO_2 and so has a higher proportion of silica rich sediment and occurs at Locations 2 and 3, but mainly in SOW13 between 943 and 945 m. This litho-unit is referred to as sil-calcrete based both on relative composition and matrix epigenesis (Nash and Shaw, 1998). Litho-unit 4 (LU4) is banded between <10 wt.% calcite and 78–95 wt.% SiO_2 and is therefore composed mainly of siliceous sediment, including silcrete and occurs entirely along the 943–945 m strandline at SOW7A and SOW13 (Table 4).

Average proportions of low-quantity major elements per litho-unit are shown in Fig. 6, from which minimal amounts of P_2O_5, MnO and Cr_2O_3 are omitted. Trends mainly show increasing MgO and an increase in the Mg/Ca ratio towards the calcite rich litho-units (i.e., towards LU1). The dominant major element after $SiO_2/CaCO_3$ is MgO which is particularly high in LU2 samples. These are relatively rich in dolomite while LU1 samples show relatively high proportions of sepiolite and palygorskite (cf. Table 2). This contrasts with the remaining low-quantity major elements all of which increase towards the more silica-rich litho-units (LU4). For instance, in LU1, the Al_2O_3 content is low between 0.67 and 1.77 wt.% and increases through the remaining litho-units to between 1.09 and 3.06 wt.% in LU2, to between 1.84 and 2.07 wt.% in LU3 and between 1.72 and 3.35 wt.% in LU4 (Table 3, Fig. 5). K_2O, Na_2O and Fe_2O_3 increase with the proportion of clay minerals and feldspars towards LU4. TiO_2 also increases towards the more SiO_2-rich litho-units (Fig. 6). These overall trends suggest that aggressive calcretisation/dolomitisation at high pH levels led to the almost complete replacement of most pre-existing silicates especially in LU1 and LU2 duricrists. The relatively high Mg/Ca ratios of these sediments suggests the prevalence of alkaline, highly evaporative conditions typified by closed basin environments. This contrasts with the apparently less intense process of silcretisation (in the LU4 and LU5 duricrusts) which in the MSB appears to take place under acidic, moderately saline conditions causing a number of the remaining silicates to survive intact. The lower than 1.2 wt.% TiO_2 content in all the litho-units infers that the mobilisation of pre-existing silicates may have been a dominant process in the pan littoral environments (Summerfield, 1982; Nash et al., 1994a,b).

6. Thin section and ESEM results

Detailed thin section and ESEM analysis was undertaken to augment geochemical and XRD data and to provide insight into complex calcretisation and especially silicification processes. Litho-clast samples were selected for this work because these usually demonstrate several stages of silicification often of an originally calcareous deposit (cf. Ringrose et al., 1999a; Nash and Shaw, 1998). ESEM investigations in low vacuum mode on subsamples from SOW1 S5 the indurated litho-clastic unit, show rounded quartz clasts with evidence of shallow etch marks closely

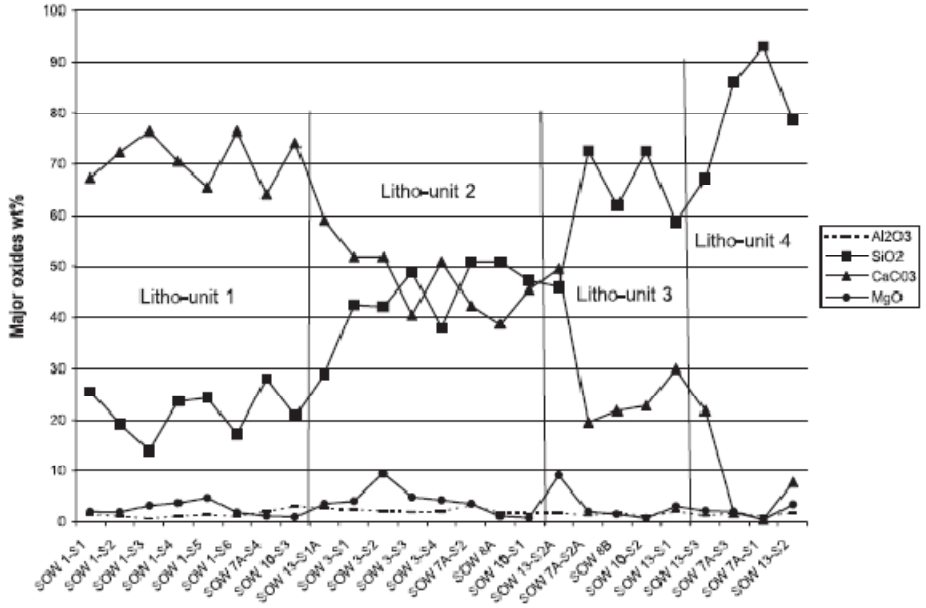

Fig. 5. Results of bulk geochemical analysis showing the subdivision of samples into four litho-units based on relative percentages of SiO_2 and $CaCO_3$. Amounts of MgO and Al_2O_3 also shown.

associated with remobilised crypto-crystalline silica in addition to laminar calcrete fragments (Fig. 7A). In this LU1 calcrete sample, EDAX results show equal proportions of Si and Ca on the remobilised surface indicating the close association of recrystallised quartz and calcite in the matrix (Table 5). The laminar calcrete appears to be relatively untouched and co-exists with remobilised amorphous silica. In a second slide (not shown), unmodified bedded Karoo sandstone clasts with circum-peripheral cracking are also evident in the mixed matrix. The SOW4 S4 sample reveals remobilised silica in the form of large and small interlayered Si plates which appear to be cracked suggesting a pressure solution mechanism (cf. Monger and Daugherty, 1991). Of particular interest are subsamples which contain bacterial mat colonies either coating siliceous plates, within small voids or occupying pre-existing organically formed casings (Fig. 7B). The casing analysed is more Si rich than the background silcrete plates implying that bacteria were sequestering Si initially from the void lining or casing (Table 5). The cocci infill and individual cocci are further enriched in Si relative to background and casing compositions while the cocci themselves also show traces of Ti not present in the background sample (Table 5). Once initiated, bacterial growth appears to be uniform with identifiable mound and chain patterns. Individual cocci are normally rounded and about 5–6 μm in diameter although some appear to be stunted or truncated (Fig. 7C).

Thin section analysis of a lensoid shoreline sample from SOW 10 terrazzo plates show several stages of Si recrystallisation (Fig. 4B, Table 6). ESEM analysis of a SOW10 shoreline silica plate indicates that the sample is composed of rounded quartz and calcite pseudomorphs along with rounded 'onion ring' ghost structures in an amorphous silica-rich matrix (Table 5, Fig 7D). The matrix contains between 42 and 76 wt.% cryptocrystalline Si with discrete Ti rich minerals. Close examination of a Ca-rich clast shows a transition of increasing silica content from the

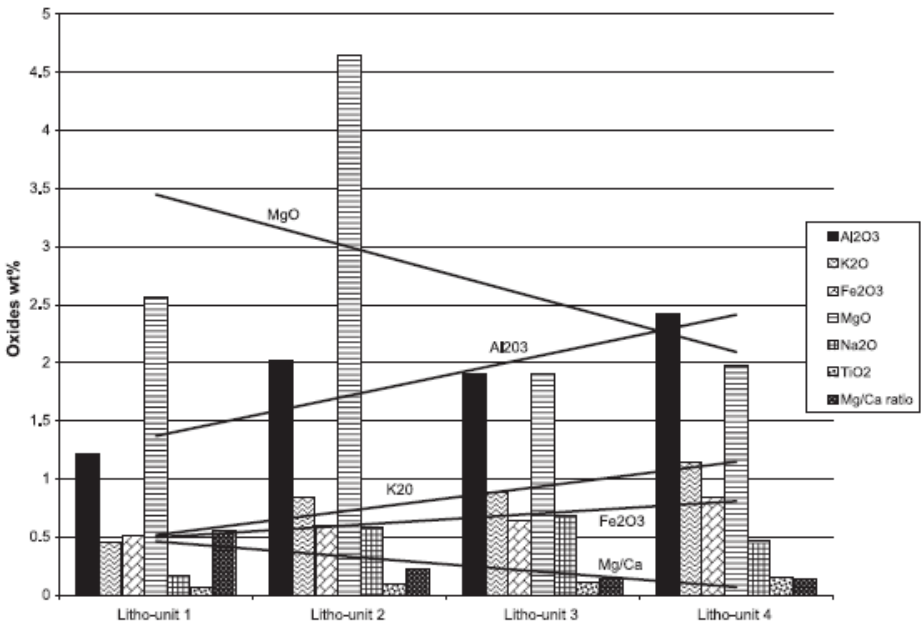

Fig. 6. Trends in the lower quantity macro-elements relative to the four litho-units showing increasing MgO and Mg/Ca ratio with increasing $CaCO_3$ (to left) and increase in remaining elements with increasing SiO_2 (to right). Elements shown on histograms from left to right are Al_2O_3, K_2O, Fe_2O_3, MgO, Na_2O, TiO_2 and the Mg/Ca ratio.

relatively Ca-rich interior out towards the Si-rich matrix (Table 5). The transition which is gradual shows a layered sequence of columnar calcite grains alternating with equiaxial calcite grains (Fig. 8A). The process seems to imply a systematic incursion (replacement) of Si-rich pore fluids into a disintegrating calcrete clast. A quartz clast with accreted calcite layers also shows impregnation with Si rich pore fluids (Table 5). The calcite layers may have transformed into a porous columnar structure prior to silica mobilisation (Fig. 8B). The 'onion ring' structures represent a more advanced stage in the process which terminates in the total replacement of clast-like shapes with matrix silica (Fig. 7D). The fact that some of the original calcite remains in what appears as matrix material may account for the apparent co-existence and inverse relationship of Ca and Si in the matrices of MSB duricrusts.

Thin section data from Location 3 (SOW13 S2 S3 units) litho-clasts shows at least three stages of crystallisation in the matrix. The matrix comprises SiO_2-rich earlier microcrystalline and later cryptocrystalline phases with accompanying voids, some of which are filled by late stage authigenic silcrete (Table 6). ESEM analysis of a nodular sample (from SOW13 S2) shows high proportions of Mg and Ca in overgrowth structures (agglomerates) developed on quartz-rich clastic sediment (Table 5). Further analysis revealed Si-rich fungal hyphae and unidentified diatoms in a Si-rich environment. Some of the hyphae occur as branching forms about 100 μm long, emplaced over interparticle voids (Fig. 8C). Others are smaller, forming stub-like growths 20 μm long or thin curvilinear forms around 30 μm in length (cf. Monger and Adams, 1996). The diatoms are also long (c. 30 μm) and fragmented in death assemblages adding silica to the littoral sediment. Both the diatoms and the hyphae suggest a wet (damp) environment during the time of deposition and both are involved in Si accumulation, suggesting that biogenic sources

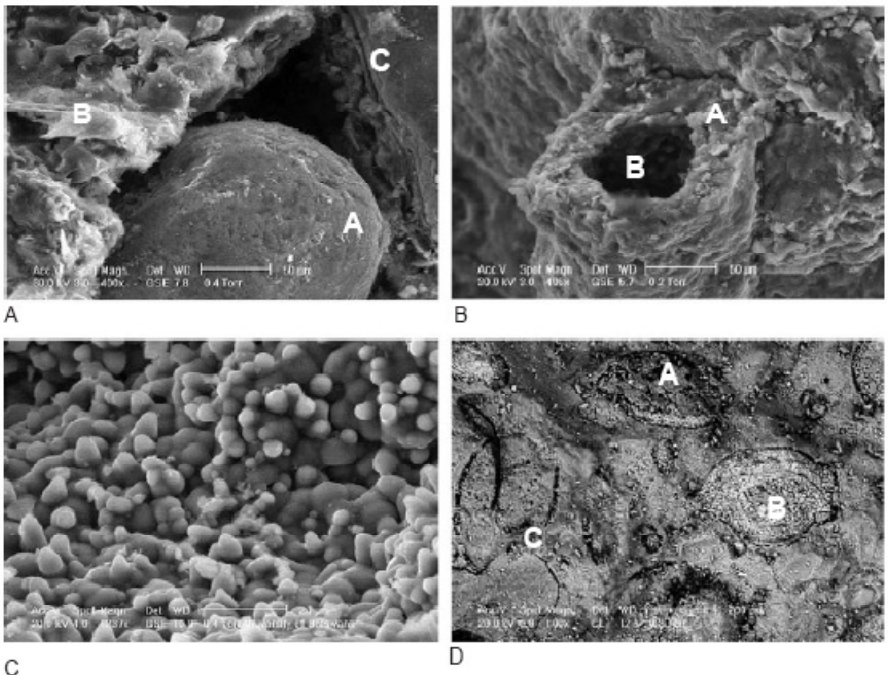

Fig. 7. (A) SEM photograph showing rounded quartz clast with evidence of shallow etch marks. (A) and remobilised silica (B) with laminar calcrete (C) in SOW1 S5 sample. (B) SEM photograph of silica-rich organic casing (A) hosting bacterial cocci coating (B) (SOW4 S4). (C) SEM photograph detail of silica-rich bacterial cocci showing developed and stunted growth forms (SOW4 S4). (D) SEM photograph showing Si rich. (A) and Ca rich (B) pseudomorphs with 'onion ring' ghost structures (C) in an amorphous silica matrix (SOW10 shoreline SiO_2 plate).

were an important factor in silica accumulation and mobilisation.

7. Thermoluminescence dating

Samples for TL dating were obtained from Locations 1 and 3. Sand grains were dated from upper and lower units at SOW1, 3 and 4, SOW7A and SOW13 (Fig. 3). Sand grains were also taken from a calcrete pit on an upper Thamalakane terrace near Maun (MaunSE12a) and from a lower terrace adjacent to the Zambezi river west of Kasane (KVFS3) to assist in providing a regional (MOZ) context (Fig. 1). The sand was obtained from older litho-clasts or rhyzoliths.

The date KVF S3 was taken from the Chobe confluence with Zambezi river and is estimated at around 493309 ± 33985 years which is a minimum age as the sample is saturated. This date tends to suggest that a lower–mid Zambezi link was reestablished during the mid-Pleistocene, inferring that direct outward drainage from the northern margin of the MOZ depression took place around this time (cf. Thomas and Shaw, 1991). Meanwhile, the MSB may have been operating as a separate basin, being infilled during major wet periods throughout the mid–late Pleistocene from the northeast, south and west (Nash et al., 1994b; Ringrose et al., 1999a, 2002a).

TL dates were obtained from samples representing different diagenetic stages within the morpho-stratigraphic units from Location 3 on PMB strandlines. The oldest approximate date in the series is from the inner portion of a rhyzolith from the lower part of SOW13 S2 (P) from which an estimated age of post

Table 5
Duricrust composition (wt.%) from samples SOW4 (4), SOW 13 (13) and SOW1 (1) from ESEM EDAX microprobe measurements

Location	Na	Mg	Al	Si	S	Cl	K	Ca	Ti	Mn	Fe
SOW1calc		13.23	4.41	36.72			0.75	43.13			1.75
SOW1calc		17.34	2.92	38.76			0.72	38.59			1.66
SOW4S4bkgd	0.58	8.41	10.33	64.75		0.72	8.92				6.28
SOW4S4casing		9.65	5.27	78.04			4.27				2.77
SOW4S4infill		4.33	5.46	82.32			4.42				3.47
SOW4S4cocci		5.29	5.16	80.84			4.8		0.36		3.55
SOW10matrix 1	1.27	0.69	1.01	41.21	0.08	0.12	0.54	1.86			0.85
SOW10matrix 2	0.9	0.69	1.18	47.19	0.11	0.07	0.58	1.28			0.46
SOW10matrix 3	2.18	1.95	2.2	76.47			1.35	3.32	0.48	0.36	1.68
SOW10Ti matrix	1.29	1.25	1.26	17.31			0.43	1.13	37.56	1.48	35.45
SOW10Sicentre	1.28	1.07	1.05	37.92	0.17	0.07	0.57	2.34	0.1		0.73
SOW10Sicol2	0.67	0.85	0.68	11.54	0.14	0.15	0.43	28.89	0.06		0.52
SOW10Sicol1	0.72	0.8	0.79	12.92	0.05	0	0.44	26.23	0.11		0.59
SOW10Simatrix	0.85	0.84	0.95	38.57	0.13	0.09	0.44	2.56			0.56
SOW10Cacol3	0.62	0.72	0.62	9.72			0.35	35.42			0.54
SOW10Cacol2	0.6	0.59	0.5	8.28			0.22	37.85			0.28
SOW10Caeqi-ax	0.68	0.95	0.78	11.62	0.05	0	0.41	27.32	0.12		0.69
SOW10Cacol1	0.6	0.72	0.68	14.12	0.12	0.11	0.35	31.46	0.2		0.55
SOW10Camatrix	0.85	0.87	0.95	36.25	0.1	0.07	0.55	3.87			0.42
SOW13agglom	1.37	14.41	4.42	57.59		3.77	2.9	12.54			
SOW13hyphae	1.66	15.85	5	50.81		4.45	3.08	16.25	0.38		5.52
SOW13ovrgrths	0.58	6.71	3.83	70.76		2.42	1.86	11.8			2.04

root calcification is given at 108 555±9017 years ago. This earliest date is partially substantiated by a similar though slightly younger date from a siliceous clast within the hardpan of SOW13 S1 which is estimated as being formed around 102 194±7621 years ago. These are the oldest recorded approximate dates on MSB upper strandlines (943–945 m) and appear to indicate the onset of a drying phase following an earlier late Pleistocene wet interval which occurred more than 110 000 years ago. Data from the Vostock core (Petit, 1999) and archeological data from Butzer (1984) and Brook et al. (1998) confirm wet conditions in the region around 120 000 years ago. Peaks in the Vostock data are constrained by ^{18}O data from drill holes off South Africa and Sea Surface Temperatures off Namibia, all of which appear to relate to Milankovitch precessional cycles (Partridge et al., 1999; Tyson et al., 2002). An estimated TL age from sand grains within a calcretised upper Thamalakane terrace northeast of Maun (MAUNSE12a) in the central MOZ (Okavango) basin gives a minimum sample age of 119 981±9850 years but could be older as it is saturated. This early wet interval may have manifested as a series of wetland areas emerging from a "lake Okavango" extending southwards and eventually overspilling into the MSB over gaps in the Gidikwe ridge (cf. Cooke and Verstappen, 1984; Thomas and Shaw, 1991; Ringrose et al., 1999a, 2002a) more than 110 000 years ago.

A second series of dates were obtained from sand grains in litho-clasts and nodules within the morpho-stratigraphic sequences at Locations 1 and 3. A siliceous litho-clast from SOW13 S3 was given an approximate TL date of 90 436±8909 years. A nodule from within the overlying nodular rhyzolith unit from SOW7A S2 was given an approximate TL age of 80 678±9202 years while a nodule from the rhyzolith free upper unit (SOW13 S2A) was dated at approximately 83 568±7898 years. Interestingly, an approximate age of 90 728±7161 years was also obtained from a litho-clast from SOW1 S6. These dates may represent the drying phase of a second wet interval which appears to have attained a similar elevation in the MSB (943–945 m) to the earlier (>110 ka) interval but which shows evidence of a later decline to the 936 m level. These dates are again consistent with Milankovitch cycles which suggest that after the 120 ka warm-wet period, less intense wet conditions recurred every 23 000 years such that a second warm, wet peak was evident around 97 ka, a third around 74 ka and a fourth

Table 6
Summary of depositional and diagenetic characteristics of major duricrust deposits of northern Sua Pan (MSB)

Duricrust type and type location	Fabric/texture	Composition	Structure	Late stage overprints
SOW 1—Calcrete (LU1 type) S20.5249 E26.3740	Clast supported hardpan-Ca and Si lithoclasts-matrix supported	Micritic low Mg calcite	Calcareous rhyzoliths, qtz clasts and calcareous lithoclasts, laminar and nodular—friable	Coated calcareous and quartz clasts.
	Replacive/displacive calcrete matrix surface Fe mottling	Microspar pore cement–secondary cements		Secondary zonation and replacement by calcite. Void formation and infill Si cocci
SOW 2–4 Calcrete with silica (LU2 type) S20.5542 E26.1686	Matrix and host fabric supported, Laminar and massive void filling cement, Microcrystalline silica overgrowths	Cryptocrystalline green silica, microcrystalline pore lining cement high Mg calcite	Massive to blocky, friable, conglomeratic, abundant rhyzoliths (8–10 cm)	Clast desiccation and cracking, coated buff silc-calc lithoclasts, concentric zonal replacement and void infilling
SOW 10 Sil-calcrete S20.3062 E25.9441	Matrix and host fabric supported, Laminar and massive void filling cement, Microcrystalline silica overgrowths	Dense cryptocrystalline (matrix and clasts) with lensoid microcrystalline crack and void infilling	Laminar massive, rounded silcrete clasts, peripherally layered with elongate silica nodules	Clast desiccation and cracking, coated silcrete lithoclasts, concentric zonal replacement, void infillings and large open voids
SOW 8A Sil-calcrete (LU2 type) S20.54361 E025.85368	Homogeneous cryptocrystalline silica	Cryptocrystalline silica with microcrystalline crack and void infilling	Massive buff siliceous lensoid pan edge nodules terrazzo type	Coated silcrete nodules, void infillings and large open voids
SOW 7A/13 (Silcrete) (LU4 type) S19.8916 E26.1390	Matrix and host fabric supported, Laminar and massive void filling cement, Microcrystalline silica overgrowths	Cryptocrystalline silica and quartz clasts with microcrystalline crack and void infilling	Massive to blocky, friable-partially consolidated abundant rhyzoliths-friable green sand	Clast desiccation and cracking, coated silcrete lithoclasts, nodular, Fe staining, void infillings and large open voids

around 51 ka in the southern African region (Tyson et al., 2002). As similar dates occur at both higher and lower strandline levels, these are therefore considered to represent the close of a major infilling and evaporative event at >80–90 ka yrs. This extended over a range of heights (from 945 to 936 m) in the MSB with the later 936 m level being more indicative of strongly evaporative conditions.

Younger dates were obtained from a siliceous lithoclast from within the nodular unit (SOW13 S2) which resulted in an estimated TL age of 41243±3033. A litho-clastic sample from SOW4 S4 was also approximately dated at 43 408±4443 years. These two dates imply a third Late Pleistocene wet interval which spanned an even wider range of heights (from 943–945 to 911 m) as it dried out in the MSB around 41000 years ago. While higher palaeo-lake levels may have extended into MOZ depression, serious closed basin conditions may be inferred from the 924–911 m strandline duricrusts which fall within the LU2 high MgO type (Fig 5). The >41–43 ka palaeo-lake event to some extent confirms earlier ^{14}C dating (c. 41 ka) previously described in the MSB by Cooke (1975), Cooke and Verstappen (1984), Shaw and Cooke (1986), Shaw and Thomas (1988) and Thomas and Shaw (1993, 2002). The 41 ka wet interval is in general agreement with isotopic data from southern Botswana (e.g., Holmgren et al., 1995).

A sample from Location 2, SOW8A taken from a shoreline siliceous, lensoid nodule was TL dated at approximately 8753±931 years. This date largely corresponds to the last major drying interval within the MSB, an episode which infers open basin conditions as freshwater from rivers to the west probably entered the lake during this episode, in a similar way to the ephemeral river inflow which

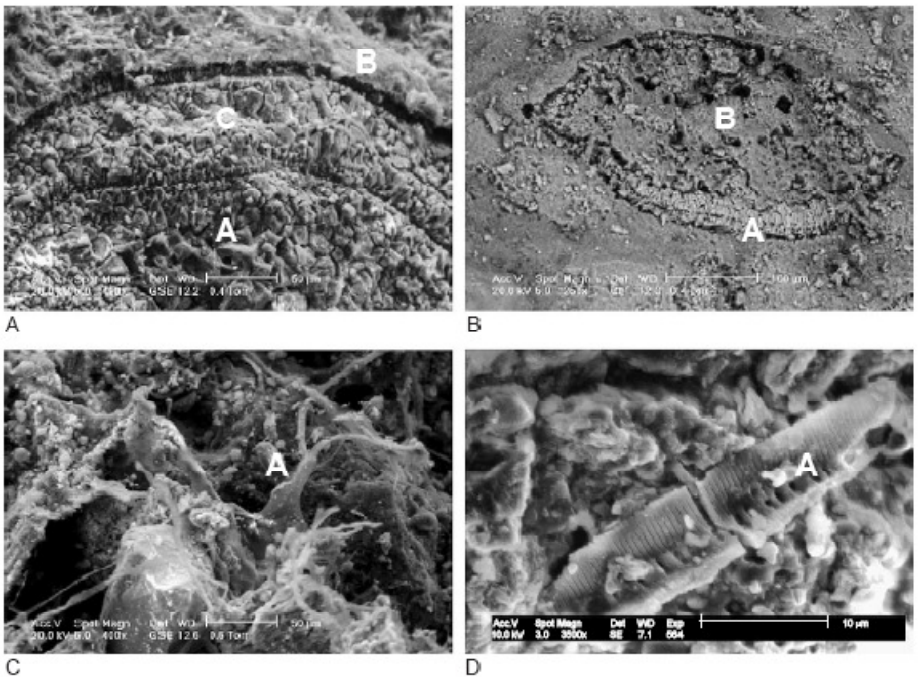

Fig. 8. (A) SEM photograph of Ca-rich clast showing transition stages from Ca-rich interior (A) out towards the Si-rich matrix (B) through a layered sequence of columnar and equiaxal calcite (C). (SOW10 shoreline SiO_2 plate). (B) SEM photograph of a Si-rich clast (B) with accreted columnar calcite (A) inferring impregnation with Si–rich matrix silica (SOW10 shoreline SiO_2 plate). (C) SEM photograph of Si-rich fungal hyphae (A) emplaced over interparticle voids (SOW13 S2). (D) SEM photograph of Si-rich diatoms (A) about 30 μm from a fragmented death assemblage (SOW7A S2).

occurs today (Shaw et al., 1997). The post 40 ka period saw a continuation of the calcification processes in an evaporative transgressive–regressive environment to c. 8 ka with almost complete drying to the present day (cf. Rust et al., 1984; Scott, 1993). The date from the pan edge environment suggests that the ultimate drying phase of the Makgadikgadi complex commenced towards the close of the Holocene altithermal (Partridge et al., 1997).

8. Discussion and conclusions

Morpho-stratigraphic and geochemical evidence developed in this work imply that both open and closed basin conditions were prevalent in the MSB throughout the Late Pleistocene mainly as a result of alternating wet and dry climatic intervals. Events described above imply that early freshwater episodes which probably resulted from regional wet events were followed by extensive drying as indicated by freshwater followed by multiple Mg-calcrete dominated phases. Later and repeated silcretisation appears to have taken as a result of more localised increases in the groundwater table when the normally saline groundwater was diluted by rain or river inflow. New evidence suggests three palaeo-lake events in the MSB, two of which precede earlier recorded wet intervals in Botswana. While the three phases are represented by duricrusted strandlines at present heights above sea level of 943–945 m, 936 m and 924–910 m, evidence from TL dates suggests that

more than one elevation was occupied at least during the two later palaeo-lake events. The last major palaeo-lake event recorded here is comparable to existing ^{14}C dates at c 41000 BP mainly from the western margin of the MSB (Cooke, 1975; Cooke and Verstappen, 1984; Shaw and Cooke, 1986; Shaw and Thomas, 1988). The range of strandline heights with similar dates may result from palaeo-lake levels moving rapidly and frequently forming transgressive/regressive cycles (Eugster and Maglione, 1979) during sustained drying.

The Late Pleistocene lake margin littoral environment and associated pore water seepage resulted in morpho-stratigraphic evidence reflecting multi-cyclic geochemical overprinting at all strandline levels. Early biogenic related calcretisation in Locations 1 and 3 followed the development of freshwater rhyzoliths in an earlier, open lake system. Later calcretisation events appear to result from the effect of various controls on calcite dissolution and precipitation in littoral pore waters during drying phases leading to saturation with respect to calcium and magnesium ions in the presence of bicarbonate. The ionic content of the major palaeo-lakes is assumed to have been introduced in solution from the catchment area (cf. McCarthy and Ellery, 1995). Saturation may have been a local, littoral effect induced in part biogenically (by macrophyte photosynthesis) and probably also by the slow loss of CO_2 by degassing (Eugster and Kelts, 1983). Biogenically and/or climatically induced precipitation took place as pore waters attained a pH level of >9. Calcite precipitated along with some dolomite as the ultimate nature of the carbonate phase was controlled by the Mg/Ca ratio of the water (Muller et al., 1972; Folk, 1974; Goudie, 1983). This may have been synchronous with the formation of sepiolite and/or palygorskite which Watts (1980) indicates occurs during or immediately after calcite or dolomite precipitation. Higher MgO levels were found both in the 943–945 m and lower sequence (936–911 m) strandlines suggesting that closed basin type evaporative conditions occurred several times. Calcretisation of littoral sands appears to have been effected as the replacement of pre-existing silicates such that very low quantities of major elements (relative to the more silicified units) remain in the calcareous units. The extensive nature of the early calcareous strandline remnants infers that closed basin conditions were prevalent over long time spans suggesting long-term tectonic stability and consistent drying. At Locations 1 and 3, the biogenic phase appears to have been followed by nodular (littoral) calcrete formation and is succeeded by major desiccation intervals, indicated by calcareous silt units in SOW1 and SOW4. The desiccation intervals suggest extensive drying around the palaeo-lakes following calcretisation.

Intermittent silification of earlier calcrete phases is the most widespread event in the strandline duricrusts and varies from silicified litho-clasts and nodules in Location 1 to the complete silicification of already silicified litho-clasts and nodules in Locations 2 and 3. Silicified duricrust units appear to be related to relatively minor rainfall or inflow events which increased the level of the groundwater table, maybe forming localised shallow palaeo-lakes. The geochemistry of the groundwater more closely resembled present-day $Na–CO_3–SO_4–Cl$-type brines. Silification typically involves a number of mechanisms including mobilisation, transport and precipitation (Smale, 1973; Summerfield, 1982, 1983a, b; Chadwick et al., 1987a, b; Thiry et al., 1988; Borger et al., 2004). Petrographic studies indicate that multiple episodes of silicification are relatively common in semiarid areas, particularly in the Kalahari environment (e.g., Summerfield, 1982, 1983c; Arakel et al., 1989; Nash et al., 1994a, b). The inverse relationships of the major oxides (high $CaCO_3$/low SiO_2) normally infers a semi-continuous process whereby at >pH 9, calcite precipitation takes place thereby lowering the pH and enabling SiO_2 to go into solution in the pore water and begin to occupy interstitial voids and cracks in the pre-existing duricrust (Gwosdz and Modisi, 1983; Ringrose, 1996; Nash, 1997; Nash and Shaw, 1998). However, this effect practically discounts the salinity factor which is particularly prevalent in the warm, shallow littoral zone of semiarid lakes where declines in near shore lakewater are associated with groundwater seepage. Recent work by Sauer and Straht (2004) shows that in semiarid (wet) lacustrine environments, enhanced evaporation leads to a lowering of the pH and the development of a geochemical barrier which leads to the polmerisation and precipitation of silica. This process also effects the reduction and depletion of the major elements due to intense leaching while facilitating the concentration

of TiO_2 (Watts, 1970). Work in Australia shows that most variation in silica concentration is explained by pH and EC values (Lee, 2003). Conclusions indicate that lower pH and less saline groundwater (pH 2.8–3.99) contains higher concentrations of dissolved silicon than relatively higher pH (6–7.18) more saline groundwater. Acidic, moderately saline groundwater is in near equilibrium with respect to amorphous silica whereas near neutral, saline groundwater corresponds to undersaturated conditions. Hence, silica in various forms may precipitate whenever Si saturation is reached and the required changes in pH may be inherent in the littoral groundwater and may not necessarily occur as a direct result of calcite precipitation (cf. Williams et al., 1985; Monger and Adams, 1996). However, the two oxides are covariant in the MSB which implies that even under different lake water geochemical conditions, the degree (or intensity) of silification varies proportionally with the $CaCO_3$ content implying preferential replacement of calcite with remobilised silica. Silica appears to enter the groundwater through the dissolution of quartz grains affected in part by a sloughing-off process. The sloughed-off silica appears to recrystallise close to the site of dissolution as cryptocrystalline silica while also forming matrix silica involved in the replacement of calcite clasts. Much of this process may be enhanced by (inter alia) diatoms, bacteria and algal growth which are active in Si uptake in the moist pan littoral. Shaw et al. (1990) and Harrison and Shaw (1995) also describe almost pure silcrete forming contemporaneously in a hyper-saline pit near Sua Pan by silica fixing cyanobacteria. Evidence from this work suggests that the abundant silica, often in the form of silcrete in the MSB is also the result of in situ silica precipitation under acidic, moderately saline pore water conditions along the pan edges.

Given the evidence presented in this work, it is likely that both exogenic (freshwater incurions) and biogenic agencies were responsible for the extensive silcretisation in the MSB littoral duricrusts. Silicification episodes appear to postdate early relatively freshwater palaeo-lake stages (with macrophyte growth) and subsequent calcretisation in multiple stages after palaeo-lake events as a result of watertable fluctuations in a semiarid environment similar to that occurring in Botswana at present (Bhalotra, 1987). The repetition of silica mobilisation through time may be responsible for prevalent SiO_2 increases up-profile. The apparent lack of intense silica remobilisation at the SOW1 (936 m) level suggests that elevated water table levels remained for a shorter duration at this height. As generally the similar water table levels (945–943 m, 924 m, 910 m) were involved in repeated SiO_2 remobilisation events over the 110 ka record, it is possible that the MSB was tectonically stable during at least the Late Pleistocene after initial faulting in the Late Tertiary.

Acknowledgements

The authors wish to acknowledge financial assistance from the University of Botswana, Research and Publications Committee (Grant RPC 509). The assistance was given in response to a request from the local SAFARI, 2000 committee for funding to consider Botswana palaeo-environments in the context of global climatic change. Soda Ash Botswana are thanked for allowing access to Sua Spit.

References

Aitken, M.J., 1985. Thermoluminescence dating. Academic Press Publishers, London.

Alonso-Zarza, A.M., Sanchez-Moya, Y., Bustillo, M.A., Sopena, A., Delgado, A., 2002. Silification and dolomitization of anhydrite nodules in argillaceous terrestrial deposits: an example of meteoric-dominated diagenesis from the Triassic of central Spain. Sedimentology 49, 303–317.

Arakel, A.U., Jacobson, G., Salehi, M., Hill, C.M., 1989. Silicification of calcrete in palaeodrainage basins in the Australian arid zone. Aust. J. Earth Sci. 36, 73–89.

Baillieul, T.A., 1979. A reconnaisance survey of the cover sands in the Republic of Botswana. J. Sediment. Petrol. 45, 494–503.

Bhalotra, Y.P.R., 1987. Climate of Botswana: Part II. Elements of climate, rainfall. Department of Meteorological Services Ministry of Works and Communication, Gaborone, Botswana (21pp.).

Blumel, W.D., Eitel, B., Lang, A., 1998. Dunes in southeastern Namibia: evidence for Holocene environmental changes in the southwestern Kalahari based on thermoluminesence data. Palaeogeogr. Palaeoclimatol. Palaeoecol. 138, 139–149.

Borger, H., McFarlane, M.J., Ringrose, S., 2004. Processes of silicate karstification associated with pan formation in the Darwin–Koolpinya area of northern Australia. Earth Surf. Proc. Landf. 29 (359), 371.

Botter-Jensen, L., Duller, G.T., 1992. A new system for measuring optically stimulated luminescence from quaternary samples. Nucl. Tracks Radiat. Meas. 20, 202–205.

Brook, G.A., Cowart, J.B, Brandt, S.A., 1998. Comparison of Quaternary environmental change in eastern and southern Africa using cave speleotherm, tufa and rock shelter sediment data. In: Alsharan, A., Glennie, K.W., Wintle, G.L., Kendall, G.C. (Eds.), Quaternary Deserts and Climate Change. Balkema, Rotterdam, pp. 239–250.

Butzer, K.W., 1984. Archeogeology and Quaternary environment in the interior of southern Africa. In: Klein, R.G, Balkema, A.A. (Eds.), Southern African Prehistory and Paleoenvironments. A.A. Balkema, Rotterdam, pp. 1–64 (Chap. 1).

Carl, C., 1987. Investigations of U series disequilibria as a means to study the transport mechanism of uranium in sandstone samples during weathering. Uranium 3, 285–305.

Chadwick, O.A., Hendricks, D.M., Nettleton, W.D., 1987a. Silica in duric soils: I. A depositional model. Soil Sci. Soc. Am. J. 51, 975–982.

Chadwick, O.A., Hendricks, D.M., Nettleton, W.D., 1987b. Silica in duric soils: II. Mineralogy. Soil Sci. Soc. Am. J. 51, 982–985.

Cooke, H.J., 1975. The paleoclimatic significance of caves and adjacent landforms in the Kalahari of western Ngamiland, Botswana. Geogr. J. 141, 430–444.

Cooke, H.J., 1979. The origin of the Makgadikgadi Pans. Botsw. Notes Rec. 11, 37–42.

Cooke, H.J., 1980. Landform evolution in the context of climatic changes and neotectonics in the middle Kalahari of north-central Botswana. Trans. Inst. Br. Geogr., NS 5, 80–99.

Cooke, H.J., Verstappen, H.Th., 1984. The landforms of the western Makgadikgadi basin in northern Botswana, with consideration of the chronology of the evolution of Lake Palaeo-Makgadikgadi. Z. Geomorphol. N.F.Bd28, Heft 1, 1–19.

Du Toit, A.L., 1933. Crustal movements as a factor in the evolution of South Africa. S. Afr. J. Sci. 24, 88–101.

Eugster, H.P., Hardie, L.A., 1978. Saline lakes. In: Lerman, P. (Ed.), Chemistry, Geology and Physics of Lakes. Springer-Verlag, New York, pp. 273–293.

Eugster, H.P., Kelts, K., 1983. Lacustrine chemical sediments. In: Goudie, A.G., Pye, K. (Eds.), Chemical Sediments and Geomorphology: Precipitates and Residua in the Near Surface Environment. Academic Press, London, pp. 321–368.

Eugster, H.P., Maglione, G., 1979. Brines and evaporites of the Lake Chad basin, Africa. Geochim. Cosmochim. Acta 43, 973–981.

Folk, R.L., 1974. The natural history of crystalline calcium carbonate: effect of magnesium content and salinity. J. Sediment. Petrol. 44, 40–53.

Geological Survey of Botswana, 2000. Geological map of the Republic of Botswana. Geological Survey of Botswana, Lobatse, Botswana (digital edition).

Goudie, A.S., 1983. Calcrete. In: Goudie, A.G., Pye, K. (Eds.), Chemical Sediments and Geomorphology: Precipitates and Residua in the Near-surface Environment. Academic Press Publishers, London.

Gumbricht, T., McCarthy, T.S., Merry, C.L., 2001. The topography of the Okavango Delta Botswana, and its tectonic and sedimentological implications. S. Afr. J. Geol. 104, 243–264.

Gwosdz, W., Modisi, M.P., 1983. The carbonate resources of Botswana. Botsw. Geol. Surv. Miner. Resour. Rep. 6 (Lobatse, Botswana, 48pp.).

Harrison, C.C., Shaw, P.A., 1995. Bacterial involvement in the production of silcretes? Bull. Inst. Oceanogr. (Monaco) 14, 291–295.

Holmgren, K., Karlen, W., Shaw, P., 1995. Palaeoclimatic significance of the stable isotopic composition and petrology of a late Pleistocene stalagmite from Botswana. Quat. Res. 43, 320–328.

Huaya, L., Xiaoyong, W., Haizhou, M., Hongbing, T., Vandenberghe, J., Xiaodong, M., Zhen, L., Youbin, S., Zhisheng, A., Guangchao, C., 2004. The plateau monsoon variation during the past 130 kyr revealed by loess deposit at northeast Qinghai-Tibet. Glob. Planet. Change 41, 207–214.

Klappa, C.F., 1980. Rhizoliths in terrestrial carbonates: classification, recognition, genesis and significance. Sedimentology 27, 613–629.

Krumbein, W.C., Garrels, R.M., 1952. Origin and classification of chemical sediments in terms of pH and oxidation–reduction potentials. J. Geol. 60, 1–33.

Lee, S., 2003. Groundwater geochemistry and associated hardpans in southwestern Australia. In: Roach, I.C. (Ed.), Advances in Regolith. CRC LEME, Curtin University of Technology, Western Australia, pp. 254–258.

Mallick, D.I.J, Habgood, F., Skinner, A.C., 1981. A geological interpretation of Landsat imagery and air photography of Botswana. Overseas Geol. Miner. Resour. Lond. 56, 1–36.

McCarthy, T.S., Ellery, W.N., 1995. Sedimentation on the distal reaches of the Okavango fan, Botswana, and its bearing on calcrete and silcrete (ganister) formation. J. Sediment. Res., Sect. A Sediment. Pet. Proc. 65 (1), 77–90.

Modisi, M.P., Atekwana, E.A., Kampunzu, A.B., Ngwisanyi, T.H., 2000. Rift kinematics during the incipient stages of continental expansion: evidence from the nascent Okavango rift basin, northwest Botswana. Geology 28, 939–942.

Monger, H.C., Adams, H., 1996. Micromorphology of calcite–silica deposits. Soil Sci. Soc. Am. J. 60, 519–530.

Monger, H.C., Daugherty, L.A., 1991. Pressure solution: possible mechanism for silicate grain dissolution in a petrocalcic horizon. Soil Sci. Soc. Am. J. 55, 1625–1629.

Moore, A.E., Larkin, P., 2001. Drainage evolution in south-central Africa since the breakup of Gondwana. S. Afr. J. Geol. 104, 47–68.

Muller, G., Irion, G., Forstner, U., 1972. Formation and diagensis of inorganic Ca–Mg carbonates in a lacustrine environment. Naturwissenschaften 59 Jg. 4, 158–164.

Nash, D.J., 1997. Groundwater as a geomorphic agent in drylands. In: Thomas, D.S.G. (Ed.), Arid Zone Geomorphology: Process, Form and Change in Drylands. John Wiley Publishers, Chichester.

Nash, D.J., Shaw, P.A., 1998. Silica and carbonate relationships in silcrete–calcrete intergrade duricrusts from the Kalahari desert of Botswana and Namibia. J. Afr. Earth Sci. 27, 11–25.

Nash, D.J., Thomas, D.S.G., Shaw, P.A., 1994a. Siliceous duricrusts as palaeoclimatic indicators: evidence from the Kalahari desert of Botswana. Palaeogeogr. Palaeoclimatol. Palaeoecol. 112, 279–295.

Nash, D.J., Shaw, P.A., Thomas, D.S.G., 1994b. Duricrust development and valley evolution: process–landform links in the Kalahari. Earth Surf. Process. Landf. 19, 279–317.

Partridge, T.C., Maud, R.R., 2000. The Cenozoic of southern Africa. Oxford University Press, New York (406 pp.).

Partridge, T.C., Demenocal, P., Lorentz, S.A., Paiker, M.J., Vogel, J.C., 1997. Orbital forcing of climate over South Africa: a 200,000-year rainfall record from Pretoria Salt Pan. Quat. Sci. Rev. 16, 1125–1133.

Partridge, T.C., Scott, L., Hamilton, J.E., 1999. Synthetic reconstructions of southern African environments during the Last Glacial Maximum (21–28 kyr) and the Holocene Altithermal, (8–6 kyr). Quat. Int. 57/58, 207–214.

Petit, J.R., 1999. Climate and atmospheric history of the past 420000 years from the Vostock ice core Antarctica. Nature 399, 429–436.

Radtke, U., Janotta, A., Hilgers, A., Murray, A., 1999. The potential of OSL and TL for dating late-glacial and Holocene dune sands tested with independent age controls of the Laacher See tephra (12,880a) at the section Mainz–Gonsenheim. 9th International Conference on Luminescence and ESR dating (LED99), Rome.

Republic of Botswana, 2000. Makgadikgadi Pans Development Plan. National Conservation Strategy Implementing Agency. Gaborone, Botswana (211 pp.).

Ringrose, S., 1996. The geomorphological context of calcrete depositions in the Dalmore Downs area, Northern Territory Australia. J. Arid Environ. 33, 291–307.

Ringrose, S., Downey, B., Genecke, D., Sefe, F., Vink, B., 1999a. Nature of calcareous deposits in the western Makgadikgadi basin, Botswana. J. Arid Environ. 43, 375–397.

Ringrose, S., Lesolle, D., Botshorna, T., Gopolang, B., Vanderpost, C., Matheson, W., 1999b. An analysis of vegetation cover components in relation to climatic trends along the Botswana Kalahari Transect. Botsw. Notes Rec. 31, 33–52.

Ringrose, S., Kampunzu, A.B., Vink, B., Matheson, W., Downey, W., 2002a. Origin and palaeo-environments of calcareous sediments in the Moshaweng dry valley, southeast Botswana. Earth Surf. Proc. Landf. 27, 591–611.

Ringrose, S., Huntsman-Mapila, P., Kampunzu, A.R., Matheson, W., Downey, W.S., Vink, B., 2002b. Geomorphological evidence for MOZ palaeo-wetlands in northern Botswana; implications for wetland change. Presentation to Monitoring of Tropical and Sub-tropical Wetlands Conference, December 2002, Maun, Botswana, Published by HOORC and the University of Florida, Centre for Wetlands.

Rust, U., Schmidt, H., Dietz, K., 1984. Palaeoenvironments of the present day arid southwestern Africa 30000–50000BP: results and problems. Palaeoecol. Afr. 16, 109–148.

Sauer, D., Straht, K., 2004. Formation of calcretes and silcretes in the Alentejo (Portugal) and consequences for the landscape, ecosystems and land use. http://www.bodenkunde.ini-freiburg.de/eurosoil/abstracts/id256_Sauer.pdf.

SAFARI2000 website. 2000. http://www.safari.geop.virginia.edu.

Scott, L., 1993. Palynological evidence for late Quaternary warming episodes in Southern Africa. Palaeogeogr. Palaeoclimatol. Palaeoecol. 101, 229–235.

Shaw, P., Cooke, H.J., 1986. Geomorphic evidence for the late Quaternary palaeoclimates of the middle Kalahari of northern Botswana. Catena 13, 349–359.

Shaw, P.A., Thomas, D.S.G., 1988. Lake Caprivi: a late Quaternary link between the Zambezi and middle Kalahari drainage systems. Z. Geomorphol. 32, 329–337.

Shaw, P.A., Cooke, H.J., Perry, C.C., 1990. Microbalitic silcretes in highly alkaline environments: some observations from Sua Pan, Botswana. S. Afr. J. Geol. 93 (5/6), 803–808.

Shaw, P.A, Stokes, S., Thomas, D.S.G., Davies, F., Holmgren, K., 1997. Palaeoecology and age of a Quaternary high level lake in the Makgadikgadi basin of the middle Kalahari. S. Afr. J. Sci. 93, 273–277.

Smale, D., 1973. Silcretes and associated silica diagenesis in southern Africa and Australia. J. Sediment. Petrol. 43, 1077–1089.

Smith, R.A., 1984. Lithostratigraphy of the Karoo stratigraphy in Botswana. Botsw. Geol. Surv. Bull. 26 (Botswana Geological Survey, Government of Botswana, Lobatse, Botswana, 34 pp.).

Summerfield, M.A., 1982. Distribution, nature and probable genesis of silcrete in arid and semi-arid southern Africa. In: Yalon, D.H. (Ed.), Aridic soils and geomorphic processes, Catena Supplement, vol. 1, pp. 37–65.

Summerfield, M.A., 1983a. Silcrete as a palaeoclimatic indicator: evidence from southern Africa. Palaeogeogr. Palaeoclimatol. Palaeoecol. 41, 65–79.

Summerfield, M.A., 1983b. Silcrete. In: Goudie, A.S., Pye, K. (Eds.), Chemical sediments and geomorphology. Academic Press Publishers, London, pp. 19–91.

Summerfield, M.A., 1983c. Petrography and diagenesis of silcrete from the Kalahari basin and Cape coastal zone, southern Africa. J. Sediment. Petrol. 53, 895–909.

Thomas, D.S.G., Shaw, P.A., 1991. The Kalahari Environment. Cambridge University Press Publishers, Cambridge (248 pp.).

Thomas, D.S.G., Shaw, P.A., 1993. The evolution and characteristics of the Kalahari, southern Africa. J. Arid Environ. 25, 97–108.

Thomas, D.S.G., Shaw, P.A., 2002. Late Quaternary environmental change in central southern Africa: new data, synthesis, issues and prospects. Quat. Sci. Rev. 21, 783–797.

Tyson, P.D. Fuchs, R., Fu, C, Lebel, L., Mitra, A.P. Odada, E, Perry, J., Steffen, W., Virji, H., (Eds.) 2002, Global–Regional Linkages in the Earth System, START. Springer-Verlag, New York, p.198.

Thiry, M., Ayrault, M.B., Grisoni, J., 1988. Ground water silicification and leaching in sands, example of the Fontainebleau Sand in the Paris Basin. Bull. Geol. Soc. Am. 100, 1283–1290.

Tiercelin, J.J., Lezzar, K.E, 2002. A 300 million year history of rift lakes in Central and east Africa: an updated broad review. In: Odada, E.O., Olago, D.O. (Eds.), The East African Great Lakes, Limnology, Palaeolimnology, and Biodiversity. Kluwer Academic Publishers, Dordrecht, pp. 3–60.

Vink, B., Ringrose, S., Kampunzu, A.R., 2001. The presence of magadiite and kenyaite in Sua pan, Central Botswana. Botsw. J. Earth Sci. 5, 32–34.

Walker, T.R., 1960. Carbonate replacement of detrital crystalline silicate minerals as a source of authigenic minerals in sedimentary rocks. Bull. Geol. Soc. Am. 71, 145–152.

Watts, S.H., 1970. Major element geochemistry of silcrete from a portion of inland Australia. Geochim. Cosmochim. Acta 41, 1164–1167.

Watts, N.L., 1980. Quaternary pedogenic calcretes from the Kalahari (southern Africa): mineralogy, genesis and diagenesis. Sedimentology 27, 661–686.

Williams, L.A., Parks, G.A., Crear, D.A., 1985. Silica diagenesis: 1. Solubility controls. J. Sediment. Petrol. 55, 301–311.

Wright, V.P., Tucker, M.E., (Eds.), 1991. Calcretes, Reprint Series Volume 2 of the International Association of Sedimentologists. Blackwell Scientific Publications, London (352 pp.).

Zoller, L., Pernicka, E., 1989. A note on overcounting in alpha-counters and its elimination. Ancient TL 7, 11–14.